

Chapter 19

Role of Non-uniform Dendrite Properties on Input Processing by GABAergic Interneurons

Anja Matthiä, Marlene Bartos, and Imre Vida

Abstract GABAergic interneurons in cortical circuits control the activation of principal cells and orchestrate network activity patterns, including oscillations at different frequency ranges. Recruitment of interneurons depends on integration of convergent synaptic inputs along the dendro-somatic axis; however, dendritic processing in these cells is still poorly understood.

In this chapter, we summarise our results on the cable properties, electrotonic structure and dendritic processing in “basket cells” (BCs; Nörenberg et al. 2010), one of the most prevalent types of cortical interneurons mediating perisomatic inhibition. In order to investigate integrative properties, we have performed two-electrode whole-cell patch clamp recordings, visualised and reconstructed the recorded interneurons and created passive single-cell models with biophysical properties derived from the experiments. Our results indicate that membrane properties, in particular membrane resistivity, are inhomogeneous along the somato-dendritic axis of the cell. Derived values and the gradient of membrane resistivity are different from those obtained for excitatory principal cells. The divergent passive membrane properties of BCs facilitate rapid signalling from proximal basal dendritic inputs but at the same time increase synapse-to-soma transfer for slow signals from the distal apical dendrites.

Our results demonstrate that BCs possess distinct integrative properties. Future computational models investigating the diverse functions of neuronal circuits need to consider this diversity and incorporate realistic dendritic properties not only of excitatory principal cells but also various types of inhibitory interneurons.

A. Matthiä, Ph.D. (✉) • I. Vida, M.D, Ph.D.
Cluster of Excellence NeuroCure, Institute of Integrative Neuroanatomy,
Charité Berlin, Charitéplatz 1, D-10117 Berlin, Germany
e-mail: anja.matthiae@charite.de

M. Bartos, Ph.D.
Institute for Physiology I, Albert-Ludwigs-Universität Freiburg, Hermann-Herder-Str. 7,
D-79104 Freiburg, Germany

19.1 Introduction

GABAergic inhibition is a crucial factor for proper network function in cortical circuits. The inhibitory system controls the level of neuronal excitation and the timing and frequency of discharge and plays a major factor in the generation of population activity patterns (Buzsáki 2006). A critical change in the balance of inhibition to excitation is thought to underlie many major brain disorders, such as epilepsy and schizophrenia (Lewis et al. 2005).

Inhibitory interneurons, in contrast to excitatory principal cells, are much lower in number and show a high level of heterogeneity with respect to their morphological, physiological and neurochemical properties (Ascoli et al. 2008; Freund and Buzsáki 1996). Interneurons can be classified into two main classes, preferentially innervating either the dendrites or the perisomatic region of their targets (Bartos et al. 2011). BCs are the main type of perisomatic inhibitory interneurons that innervate the soma and the proximal dendrites of principal cells and various types of interneurons. BCs are interconnected by mutually inhibitory synapses and gap junctions and are thought to play a central role in the generation of oscillations at theta (4–12 Hz), gamma (30–90 Hz) and ripple frequencies (14–200 Hz) (Bartos et al. 2007; Buzsáki and Draguhn 2004).

BCs are recruited by different mechanisms, including the tonic drive through metabotropic receptors (Whittington et al. 1995; Fisahn et al. 2002) or the phasic excitation mediated by ionotropic receptors in glutamatergic synapses (Geiger et al. 1997). With respect to circuit structure, excitatory synapses are formed by either (1) afferent pathways originating outside the area or (2) “recurrent” collaterals of local principal cells resulting in feedforward vs. feedback activation of the interneurons, respectively.

19.1.1 Circuitry of the Dentate Gyrus

In order to understand synaptic activation and integration in BCs, we need to consider the specific organisation of the surrounding network.

The dentate gyrus (DG) is considered to be the gateway to the hippocampus, the first station of the so-called “trisynaptic pathway” (Andersen et al. 1971). As a cortical area, the DG shows a strict but simple layered structure (Fig. 19.1a): the cell body layer densely packed with somata of mainly principal cells, the granule cells (GCs), also called as the granule cell layer. GC dendrites emerge from the apical pole of the soma and extend into the neuropil, the “molecular layer”, whereas the axon arises from the basal pole and extends into the “hilus”. Most interneurons, including BCs, differ from GCs in that they have a bipolar dendritic arbour with apical dendrites in the molecular layer and basal dendrites in the hilus.

The main input to the DG, the perforant path, constitutes fibres from the entorhinal cortex and terminates in the outer two-thirds of the molecular layer forming synapses onto distal dendrites of GCs as well as inhibitory interneurons

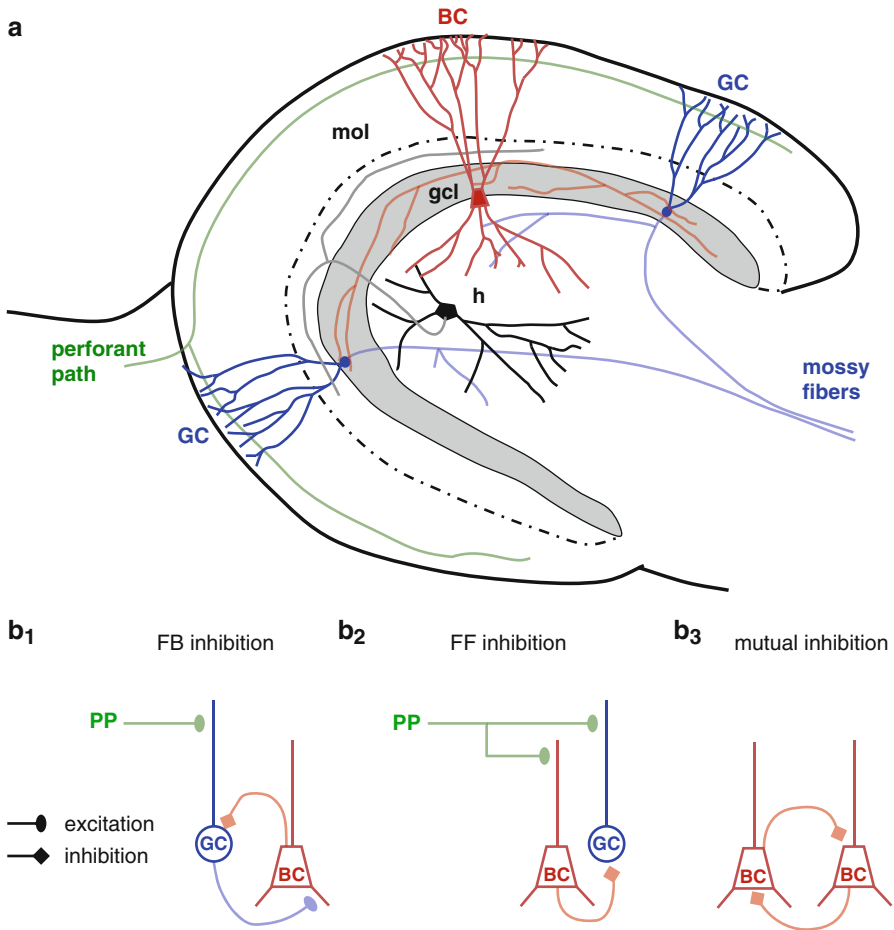


Fig. 19.1 The dentate gyrus circuitry. (a) The granule cell layer with the densely packed somata of granule cells (GC, blue) is shown in grey. These cells are activated mainly by distal excitatory perforant path synapses (in green) but also from excitatory mossy cells (black). Granule cell axons form the mossy fibres with local collaterals in the hilus. Basket cells (BC, red) have a larger cell body located at the border of the granule cell layer (gcl) to the hilus (h). The apical dendrites of basket cells, similar to those of granule cells, extend into the molecular layer (mol) that is subdivided into an outer and inner part (indicated by the dashed line). Basket cell dendrites receive distal synaptic input from the perforant path and proximal input from mossy cells within the inner molecular layer. In contrast to granule cells basket cells have basal dendrites which extend into the hilus and receive recurrent excitatory input from granule cells. (b) Schematic representations of connectivity between perforant path (PP), basket cells and granule cells. BCs are involved in feedback (FB, b₁) or feedforward inhibition (FF, b₂). At the same time they are interconnected by mutual inhibitory synapses (b₃). Whereas FF inhibition is generated by the afferent activation of BCs, FB inhibition involves the activation of GCs

(Amaral 1993). Dendrites in the inner third of the molecular layer are targeted by commissural/associational fibres originating from excitatory mossy cells in the ipsi- and contralateral hilus. Thereby, dendritic trees of GCs and interneurons receive strictly laminated, segregated inputs (see Förster et al. 2006).

The main output of the DG is conveyed by the mossy fibres, i.e., GC axons being directed to the hilus and the CA3 area. Within the hilus, mossy fibres form axon collaterals contacting basal dendrites of DG interneurons and thereby provide direct excitatory feedback. Thus, many DG interneurons, including BCs, receive input from both afferent pathways and recurrent collaterals, and therefore they are embedded in both feedforward and feedback inhibitory microcircuits (Fig. 19.1b).

19.1.2 Integrative Properties of Dendrites

The dendritic tree of a neuron receives excitatory and inhibitory synaptic inputs. These inputs are transmitted along the dendro-somatic axis until they reach the perisomatic domain and the site of action potential initiation, typically at the axon initial segment. How different types of inputs are integrated to produce specific neuronal output is dependent on the spatio-temporal pattern of inputs (Magee 2000), the morphological structure of the cell (Rall 1959; Vetter et al. 2001) and the membrane properties (Gulledge et al. 2005).

Integrative membrane properties can be determined by passive and active mechanisms. Passive membrane properties together with the morphology define the electrotonic structure of neurons (Rall 1959, 1962) and therefore set the basis for integration of synaptic signals within the dendritic tree. Integration or summation of different inputs over time is enhanced when the cell membrane has low leak conductance and the intracellular (“axial”) conductance (Spruston et al. 2008) is high. As an effect, the integration time window becomes larger, and many inputs from different sources, e.g. different brain regions, can be integrated. Thus, the cell will act as an “integrator”. In contrast, temporal summation in a neuron is smaller when the leak conductance is large. Synaptic signals would decay rapidly and show more attenuation along the dendrites, and inputs would summate only within a brief time window. These passive properties would, thus, result in a “coincidence” or a “synchrony detector” neuron. Therefore, passive membrane properties can set the basis for different modes of integration, such as strong integration (e.g. DG GC Krueppel et al. 2011) or synchrony detection (e.g. CA1 pyramidal cell Losonczy and Magee 2006).

On the basis of the passive properties, active, i.e. voltage dependent, conductances increase the cell’s repertoire of integrating synaptic inputs, for example by counteracting the passive location-dependent attenuation (Magee 2000) or compartmentalising the dendrite into different functional units (e.g. Larkum et al. 2009; Scott et al. 2005).

19.2 Dendritic Properties of Dentate Gyrus Basket Cells

The passive properties of each dendritic cable segment can be characterised by three main parameters: the specific membrane resistance R_m , the specific membrane capacitance C_m and the intracellular (axial) resistivity R_i . R_m describes the leakiness

of the membrane and is determined by the presence of leak channels in the membrane. C_m is a measure of the capacitive nature of the membrane. The lipid and protein content is the main determinant of the dielectric attributes of the membrane and thus C_m . Finally, R_i reflects the resistive properties of the intracellular medium, and it may change depending on the intracellular content, including the number and size of intracellular organelles and the fluidity of intracellular medium. Ultimately, the knowledge of R_m , C_m and R_i as well as the detailed morphological structure of a neuron makes it possible to create a realistic computational model of the cell and analyse its integrative properties either in isolation or as part of a network.

The development of a realistic model of BCs includes three major steps: (1) whole-cell patch-clamp recordings of passive voltage responses to current application; (2) visualisation and 3-dimensional reconstruction of cell morphology and (3) derivation of R_m , C_m and R_i by numerical simulations using a model based on the recorded voltage traces and the respective neuronal morphology.

Upon completion of these separate steps the developed model was used to study the integrative properties of BC dendrites. We showed that BC dendrites are optimised for speed and efficacy of signalling properties. BC dendrites exhibit faster signalling properties in basal than apical dendrites, but at the same time the efficacy of slow distal apical inputs is increased. In the final part of the chapter, we discuss the implications of BC signalling properties for the proper function of the DG circuitry.

19.2.1 Electrophysiological Experiments

In the experiments, BCs were selected in 300 μm hippocampal slices of 17–19-day-old Wistar rats on the basis of their large cell body located at the border of the granule cell layer to the hilar region. To confirm their physiological identity, a series of hyperpolarising subthreshold and depolarising suprathreshold current pulses were injected to evaluate input resistance and firing patterns under current clamp conditions. Typically, BCs show low input resistance, produce very brief action potentials followed by a large-amplitude fast afterhyperpolarisation and can discharge at very high frequencies in response to sustained current pulses (119–216 Hz at 0.75–1 nA current amplitude; at 30–34 °C; Fig. 19.2a).

To record passive responses from the neurons, ligand- and voltage-dependent currents need to be eliminated. Therefore, blockers of glutamatergic (10 μM 6-cyano-7-nitroquinoxaline-2,3-dione) and GABAergic (20 μM bicuculline or 1–2 μM gabazine) synaptic transmission and active conductances (sodium channels, 1 μM tetrodotoxin), including the hyperpolarisation-activated current (I_h , 30 μM ZD7288), were bath-applied, and voltage responses were kept as small as possible (see below, Fig. 19.2).

Electrophysiological recordings were performed with two electrodes in two different experimental configurations: (1) dual-somatic recordings and (2) dual-somatodendritic recordings (Fig. 19.2a, d). In the dual-somatic recording configuration, current injection is separated from voltage recording. Therefore, artefacts that

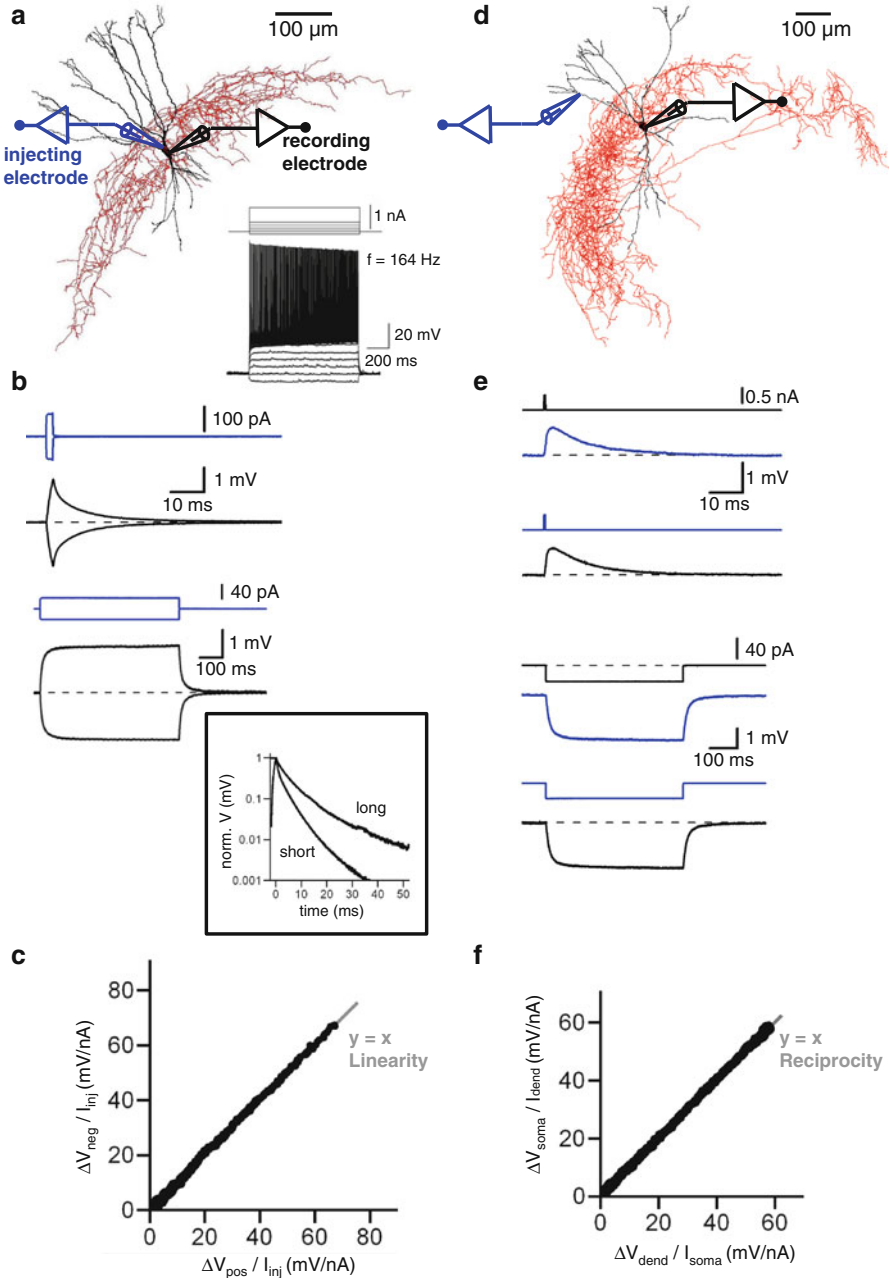


Fig. 19.2 Two-electrode recordings of passive responses to short and long current pulses. (a) Detailed reconstruction of a basket cell with a schematic representation of the dual-somatic recording configuration. Injection and recording electrodes were separated, and only voltage responses from the recording site were used for further analysis. *Inset*: Sub- and suprathreshold responses to a family of hyperpolarising and depolarising current pulses. This cell fired action potentials at $164\ \text{Hz}$ in

would emerge during current application due to series resistance and capacitance of the electrodes are eliminated from the voltage-recording electrode. This is especially important for the early, fast decay of the voltage transient in response to brief current injections. This early transient reflects a rapid redistribution of charge within the cell after the end of the current pulses. Conceptually, the intracellular medium is a low-resistance path (reflected by R_i) which enables the rapid charge redistribution before the membrane capacitance can fully discharge through the high-resistance path across the membrane (determined by R_m). In case of single-electrode recordings this transient is superimposed by electrode artefacts (Schmidt-Hieber et al. 2007; Thurbon et al. 1998; Major et al. 1994), but dual-somatic electrode configurations as in our experiments enable the reliable recording of this essential determinant of R_i .

In the second somato-dendritic recording configuration, one electrode was positioned at the soma and the other on the apical dendrite between 100 and 300 μm distance from soma (Fig. 19.2d, Nörenberg et al. 2010; Hu et al. 2010). Currents were applied to the soma, and voltage recordings were performed at both sites, somatic and dendritic (Fig. 19.2e, black and blue traces, respectively). In these recordings, the electrode artefact could not be avoided in the somatic responses, and thus the initial fast decay was excluded from analysis (see overlay of simulated and experimental traces in Fig. 19.3a). Nevertheless, voltage responses obtained from an additional point of the dendritic structure served as a spatial constraint for the derivation of the parameters R_m , C_m or R_i . This was particularly important to enable us to assess homogeneity along the somato-dendritic axis.

In both configurations, membrane properties were probed by two sets of current pulses, either long pulses with small amplitude (400–600 ms, 20–50 pA, Fig. 19.2b, e lower traces) or short pulses with large amplitude (0.5 or 2 ms, 100–500 pA, Fig. 19.2b, e, upper traces). Voltage responses to both sets of pulses were always kept smaller than 4 mV to prevent activation of voltage-dependent conductances (Fig. 19.2b, e). The advantage of the dual pulses was that the brief pulses probe membrane properties mainly locally, i.e. at the soma, whereas the long pulses can charge more distal membrane surface, and thereby the kinetics of charging and discharging phases may uncover potential inhomogeneities in R_m or C_m .

Indeed, analysing the decay of voltage responses to short and long current injections revealed a difference in the apparent membrane time constant (Fig. 19.2b, inset).

←

Fig. 19.2 (continued) response to a 1 nA current pulse. **(b)** Voltage responses (*black*) to short (*top*) and long (*bottom*) current pulses (*blue*) in the dual-somatic recording configuration. Inset: Semilogarithmic plot of the decay phase of short and long voltage responses shows their different time constants. **(c)** Point-by-point comparison between voltage responses to positive and negative current injection indicates linearity of the voltage responses. **(d)** Detailed reconstruction of a basket cell with a schematic representation of the dual-somato-dendritic recording configuration. **(e)** Voltage responses to short (*top*) and long (*bottom*) current pulses recorded from the soma (in *black*, with current injected to the dendrite in *blue*) or the dendrite (in *blue*, with current injected to the soma in *black*). **(f)** Point-by-point comparison of somatic responses to dendritic current injection, and dendritic responses to somatic current injection indicate reciprocity of the response. Reproduced with permission from Nörenberg et al. (2010)

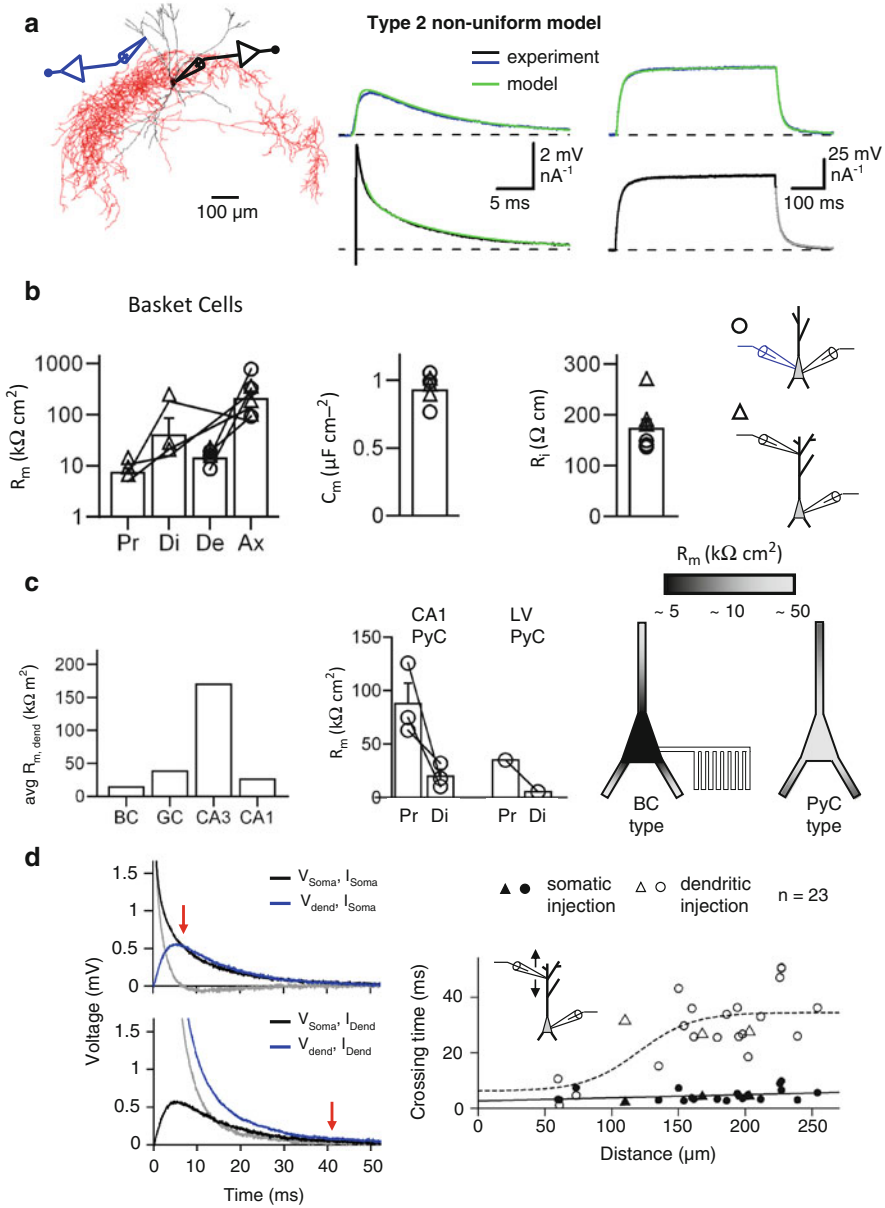


Fig. 19.3 Basket cell cable parameters in comparison to other cell's properties. (a) The best-fit parameter combination of R_m , C_m , R_i and the residual pipette capacitance resulted in a good reproduction of the experimental traces (somatic, black; dendritic, blue) in non-uniform R_m model (five parameters: $R_{m, \text{prox}}$, $R_{m, \text{dist}}$, $R_{m, \text{axon}}$, C_m and R_i). Simulated traces are shown in green. Left: Reconstruction and recording configuration for the basket cell. (b) Summary bar charts of best-fit cable parameters R_m (left), C_m (middle) and R_i (right) for six basket cells, three dual-somatic recordings (circles) and three somato-dendritic recordings (triangles). Abbr.: Pr, $R_{m, \text{prox}}$; Di, $R_{m, \text{dist}}$;

Short voltage responses decayed much faster than long voltage responses. This difference suggested that proximal and distal surface membrane areas may display differences in their passive membrane properties, more specifically a non-uniform membrane resistance.

Altogether, the combination of dual-somatic and somato-dendritic recordings and the analysis of brief and long responses can constrain R_m , C_m and R_i well, offering good estimates of these parameters.

To confirm that our recordings reflected a passive electrotonic system, dual-somatic responses were checked for linearity and somato-dendritic responses were checked for reciprocity, prerequisites for passive systems (Major et al. 1994). To test for linearity, voltage responses to positive and negative current pulses were compared. The point-by-point comparison did not show any significant deviation from the identity line (Fig. 19.2c) irrespective of whether short or long current pulses were used. To test for reciprocity, dendritic current injections were performed and the resulting somatic voltage responses were compared to the dendritic ones evoked by somatic current injections. The points did not deviate from the identity line in this test either, indicating that reciprocity held true also for our somato-dendritic recordings (Fig. 19.2f).

19.2.2 Morphological Analysis and Reconstruction

During the experiment, recorded cells were filled with biocytin and subsequently visualised for reconstruction and morphological analysis. Reconstructions were only performed of those neurons whose extensive dendritic and axonal arborisation was considered complete.

On the basis of stable electrophysiological recording conditions and the morphological criteria, six cells (three dual-soma recordings and three somato-dendritic recordings) were selected for further analysis. Full 3-dimensional reconstructions were made using a NeuroLucida reconstruction system at x63 magnification. First, the soma was traced as a closed contour by following its perimeter. Second, dendrites and axon were reconstructed as a series of virtual cylinders giving rise to a set of interconnected local compartments. Dendritic branches had larger (0.68–2.52 μm) and slowly changing diameter, whereas axon collaterals had thin diameter

←
Fig. 19.3 (continued) De, average dendritic R_m ; Ax, $R_{m, \text{axon}}$. (c) Comparison between R_m of basket cells and principal cells such as granule cells (GCs), CA3 pyramidal cells (CA3), CA1 pyramidal cells (CA1) and layer V neocortical pyramidal cells (LV PyC). (d) Somatic (black) and dendritic (blue) responses to short somatic (top left) or dendritic (bottom left) current injections. The difference between both traces is shown in grey. Note that in case of somatic injection somatic and dendritic responses cross each other at an early time point of the decay phase (6.6 ms), but both responses to dendritic injections do not cross but converge at a later time point (50.6 ms). The summary graph for all 23 somato-dendritic recordings (right) shows that this is true for all recordings with the dendritic recording site <120 μm from soma. Reproduced with permission from Nörenberg et al. (2010)

(0.32–1.33 μm at distances of 0–500 μm from soma) and regularly spaced varicosities (“boutons”). Dendrites extended either into the molecular layer or the hilus corresponding to apical or basal, respectively. In contrast, the axon arborised extensively in and near the granule cell layer. Finally, dendrites and axons could also be distinguished on the basis of their branching pattern: The angle between two children branches was narrow for dendrites ($<90^\circ$), whereas for the axon the angle between children branches could be up to 180° . Because the diameters of dendrites appeared unchanged by fixation, the reconstructed morphology was not corrected for any shrinkage.

19.2.3 Detailed Biophysical Model of BCs

To determine the three cable parameters, R_m , C_m and R_i , the reconstructed morphology was imported to the simulation environment NEURON (Hines and Carnevale 1997; Carnevale and Hines 2006) and used as the spatial framework for subsequent single-cell simulations. In the NEURON model, current pulses identical to those in the experiment were used to simulate voltage responses of the imported cell assuming certain values for R_m , C_m and R_i . These values were then systematically changed using a random-walk procedure and NEURON’s built-in Brent’s principal axis algorithm (Brent 2002) in order to best reproduce voltage responses measured in the experiments. The best fit between experimental and simulated traces was quantified by the minimal sum of their pointwise squared errors (SSE) for both short and long pulses (Fig. 19.3a).

Initially, R_m , C_m and R_i were assumed to be uniform throughout the entire cell (data not shown), but no parameter combination was found that reproduced well the difference in the decay time course of short and long pulses. Therefore, alternative models with non-uniform parameters were tested next. While no substantial improvement in SSE was found for non-uniform C_m or R_i , implementing non-uniform R_m improved the fit and reduced the SSE markedly. In the non-uniform R_m model, three domains were defined: soma/proximal dendrites ($\leq 120 \mu\text{m}$), distal dendrites ($>120 \mu\text{m}$) and axon. On average, the SSE was reduced by 84.7 % in the best-fit non-uniform model in comparison to the uniform one.

The best-fit value for C_m was $0.93 \mu\text{F cm}^{-2}$; for R_i it was $172.1 \Omega \text{ cm}$. In the final non-uniform model, R_m was low in proximal dendrites with $R_{m, \text{prox}} = 7.6 \text{ k}\Omega \text{ cm}^2$ ($x \leq 120 \mu\text{m}$) and high in distal dendrites with $R_{m, \text{dist}} = 74.3 \text{ k}\Omega \text{ cm}^2$. The highest R_m , however, was found to be in the axon ($R_{m, \text{axon}} = 281.6 \text{ k}\Omega \text{ cm}^2$; Fig. 19.3b; Nörenberg et al. 2010).

This result was in strong contrast with the non-uniformity observed in principal cells (Stuart and Spruston 1998; Golding et al. 2005). To obtain further evidence for the gradient of R_m along the somato-dendritic axis in BCs, the time course of voltage transients evoked by brief current pulses to either the dendritic or the somatic recording sites was analysed (Fig. 19.3d). Theoretically, if brief current pulses are injected into compartments with differing R_m , the voltage transients will decay more

rapidly in the low- R_m region (in our case at the BC soma) than in the high- R_m region (BC distal dendrites). This leads to a crossing of superimposed voltage responses in the two recording sites (London et al. 1999). Conversely, injecting current into the high- R_m region, local signals will decay more slowly than remote ones; thus both traces would not cross but converge to a common level at a later time point. To compare this theory with the experiment, somatic and dendritic voltage transients to short current pulses were compared in somato-dendritic recordings from BCs (Fig. 19.3d). For somatic stimulation, somatic transients showed faster decay than dendritic ones and the two transients crossed within 10 ms after the pulse (23 somato-dendritic recordings) indicating that a lower R_m region is located close to the soma. For dendritic stimulation 100 μm or more from soma, the two transients did not cross but converged to a common level.

In summary, this analysis confirmed a decreasing gradient of R_m towards the soma in BCs. The value of R_m in BCs differed substantially from values in other cell types in the hippocampus and the neocortex (Fig. 19.3c). The average dendritic R_m ($R_{m, \text{dend}} = 14.2 \text{ k}\Omega \text{ cm}^2$, in the presence of I_h channel blocker ZD 7288) was lower in BCs than in hippocampal principal cells, including GCs (Schmidt-Hieber et al. 2007), CA3 (Major et al. 1994) and CA1 pyramidal cells (Golding et al. 2005: weighted mean $R_{m, \text{dend}} = 26 \text{ k}\Omega \text{ cm}^2$, assuming a distal:proximal membrane area ratio of 2:1). Furthermore, BCs showed a gradient of R_m which decreases from distal dendrites towards the perisomatic domain, opposite to that observed in both CA1 and neocortical layer V pyramidal cells (Golding et al. 2005; Stuart and Spruston 1998).

In contrast to R_m , values for both C_m and R_i in BCs were comparable to those in other cell types in the hippocampus and the neocortex. The best-fit non-uniform model revealed a C_m of $0.93 \mu\text{F cm}^{-2}$, consistent with previous capacitive measurements of nucleated patch recordings from hippocampal neurons ($0.90 \mu\text{F cm}^{-2}$; Gentet et al. 2000). Furthermore, similar values of C_m were obtained using whole-cell recordings of GCs ($1.01 \mu\text{F cm}^{-2}$; Schmidt-Hieber et al. 2007), CA3 pyramidal neurons ($0.75 \mu\text{F cm}^{-2}$; Major et al. 1994) and CA1 pyramidal neurons ($1.50 \mu\text{F cm}^{-2}$; Golding et al. 2005). The similarity of C_m between different cell types quite plausibly suggests comparable lipid and protein composition of cellular membranes in these distinct cell populations.

The mean value of R_i in BCs was $172 \pm 18.5 \Omega \text{ cm}$. First studies of interneuron cable properties either failed to determine R_i (Chitwood et al. 1999) or obtained highly variable values ($52\text{--}484 \Omega \text{ cm}$, Thurbon et al. 1998). Early estimates of R_i in hippocampal principal cells were also more variable and higher ($160\text{--}340 \Omega \text{ cm}$, Major et al. 1994). These values were based on single-electrode recordings and were very sensitive to recording conditions, such as electrode parameters affecting the fast initial decay of voltage responses. More recent studies using a dual-electrode recording configuration, in contrast, report values of R_i in GCs ($194 \Omega \text{ cm}$; Schmidt-Hieber et al. 2007) and CA1 pyramidal neurons ($178 \Omega \text{ cm}$; Golding et al. 2005) which are closer to our estimate for BCs but markedly lower for layer 5 neocortical pyramidal neurons ($70\text{--}100 \Omega \text{ cm}$; Stuart and Spruston 1998). As R_i is highly dependent on the density of intracellular organelles as well as cytoplasmic ion concentrations, it may vary between different cell types. For example, in BCs the

density of mitochondria is higher due to a higher metabolic rate (Gulyás et al. 2006) and thus R_i could be increased. On the other hand, due to a more positive Cl^- equilibrium potential in BCs compared to principal neurons (Vida et al. 2006), the intracellular Cl^- concentration will be higher and result in a decreased R_i because of the high mobility of Cl^- (Hille 2001).

In the following section, we show what effects BC cable parameters have on synaptic integration in these cells.

19.2.4 Integration of Synaptic Inputs in Basket Cells

How are the different inputs onto apical versus basal dendrites integrated in BCs? How do these passive cable properties contribute to fast signalling?

To answer these questions, simulations were run in one single-cell model out of our sample¹ using its best-fit parameters of the non-uniform R_m model (Fig. 19.4). To better reproduce the low input resistance and the physiological conditions in BCs, a uniformly distributed I_h conductance with $6.8 \text{ pS } \mu\text{m}^{-2}$ was inserted into the membrane of the model cell. This value was chosen from the experimental measurement of input resistance of the same BC before ZD 7288 application.

To study the generation and propagation of synaptic inputs, an excitatory synapse was placed on apical or basal dendrites at different locations corresponding to the perforant path input distally, the commissural-associational path input onto proximal apical dendrites and the recurrent GC input onto basal dendrites (Fig. 19.4a, left). These synapses were modelled as conductance-based excitatory synapses with a rise time of 0.2 ms, a decay time constant of 1 ms and a reversal potential of -5 mV (Geiger et al. 1997).

Since the action potential initiation site is close to the soma (Hu et al. 2010), it is important to know how excitatory postsynaptic potentials (EPSPs) are shaped at the synapse and the soma. Figure 19.4a shows the EPSP amplitude plotted against the distance of the synapse that was activated on basal dendrites (negative x -values) or apical dendrites (positive x -values). Distal synapses evoke somatic EPSPs with small amplitude because of strong attenuation along the dendrites, whereas proximal synapses showed less attenuation and were thus larger (Fig. 19.4a, centre). Attenuation of EPSPs was similar for basal and apical dendrites, even though the local EPSP amplitude was larger for basal than for apical sites (Fig. 19.4a, right).

BCs are well known for their fast and precise timing of their intrinsic and synaptic signalling. To study temporal aspects of dendritic integration with realistic specific cable parameters, latency, decay time constant and half-duration of EPSPs were analysed (Fig. 19.4b). The latency was calculated between the onset of synapse activation and the peak of somatic EPSP waveform, and thus it is a measure of propagation velocity. Somatic EPSPs induced by inputs onto basal dendrites

¹All model BCs can be downloaded from ModelDB (#140789; <http://senselab.med.yale.edu/modeldb/>).

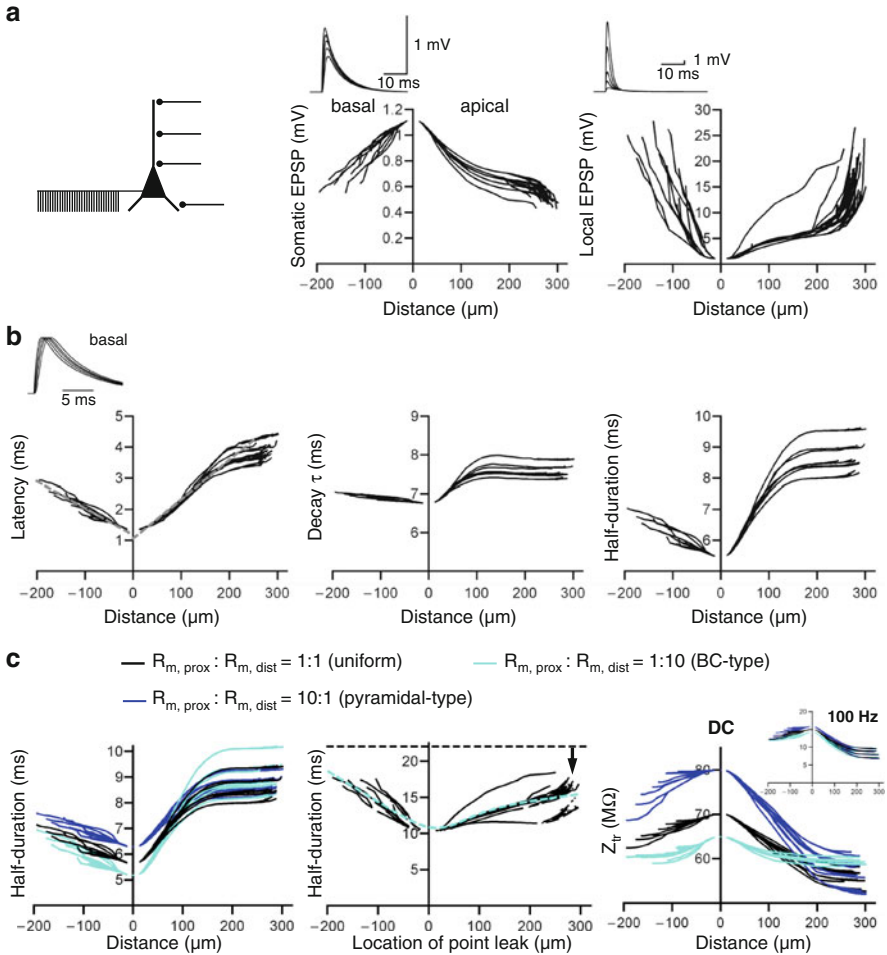


Fig. 19.4 Timing and efficacy in basket cells. **(a)** For each graph one conductance-based synapse was placed at different locations (scheme, *left*) along the somato-dendritic axis, with negative x -values for basal and positive ones for apical dendrites. For each synapse, the somatic (*middle*) and local (*right*) excitatory postsynaptic potential (EPSP) was analysed and plotted against the distance of the synaptic site from soma. **(b)** Latency (*left*), decay time constant τ (*middle*) and half-duration (*right*) of somatic EPSPs were plotted against the distance of the activated synapse from soma. Inset, *left*: Representative somatic EPSP waveforms for the activation of basal synapses at different distances from soma. **(c)** The ratio between $R_{m, \text{prox}}$ and $R_{m, \text{dist}}$ was subsequently changed from uniform (*black*) to either pyramidal type (*dark blue*) or basket cell type (*light blue*). The half-duration (*left*) and transfer resistance Z_{tr} (*right*) were then computed for the three different scenarios. Inset: Transfer impedance for 100 Hz signals. Reproduced with permission from Nörenberg et al. (2010)

showed shorter latencies than those in response to apical dendritic inputs, indicating faster signal propagation on basal dendrites ($116 \mu\text{m ms}^{-1}$ vs. $79 \mu\text{m ms}^{-1}$ for distances $\leq 200 \mu\text{m}$; Fig. 19.4b, left). Similarly, the decay of EPSPs as well as somatic EPSP half-durations were faster and shorter, respectively, for basal than for apical dendrites (Fig. 19.4b, centre and right).

In summary, the fastest somatic EPSPs were generated if the synapse is located on basal dendrites close to the soma. This difference gives a kinetic advantage to feedback over feedforward synapses (see Sect. 19.3.2).

How do the specific cable properties contribute to the fast signalling phenotype of BCs? To understand the effect of the R_m gradient in BCs on timing, we compared the effect of three different scenarios with the same cell morphology keeping the total leak conductance constant. Either no gradient was implemented, i.e. R_m was equal for all dendritic segments ($R_{m, \text{prox}}:R_{m, \text{dist}} = 1:1$), the gradient was either of the BC type ($R_{m, \text{prox}}:R_{m, \text{dist}} = 1:10$) or pyramidal cell type ($R_{m, \text{prox}}:R_{m, \text{dist}} = 10:1$). For basal and proximal apical dendrites, the BC-type gradient produced faster EPSP half-durations than the other two, the model with no gradient and the pyramidal cell-type model (Fig. 19.4c left).

However, somatic EPSP half-durations for distal apical synapses were heterogeneous, independent of which scenario was used. To systematically analyse the relation between the location of the low- R_m region and the kinetics of the somatic EPSPs, the R_m in the model with BC-type gradient was uniformly increased to the distal, high R_m and the low R_m was implemented in a single segment with varying location along the somato-dendritic axis. Activating a distal synapse (arrow in Fig. 19.4c, centre) the corresponding somatic EPSPs were the fastest if the low- R_m region was implemented close to the soma. Thus, a low somatic R_m produced the maximal EPSP speeding for distal inputs, too.

These results indicate that BC cable properties are optimised for EPSP speeding. However, a low R_m leads to stronger attenuation and thus lower efficacy of distal inputs. To study the efficacy of synaptic inputs, transfer impedance for fast inputs and transfer resistance (Z_{tr}) were computed (Fig. 19.4c, right). The transfer impedance denotes the degree of coupling between a synaptic location on the dendritic tree and the soma, i.e. the “efficacy” of signal transmission (Koch 1999). The smaller the transfer impedance the larger the attenuation, as it is the case for distal inputs, revealed in our analysis (Fig. 19.4c, right).

The BC-type non-uniform model led to an increase in Z_{tr} for distal inputs, whereas it remained low in the model with no R_m gradient (Fig. 19.4c, right). Furthermore, compared to the pyramidal cell-type non-uniformity, the BC-type model equalises Z_{tr} for all inputs along the apical dendrite. Therefore, interpreting Z_{tr} as a measure for efficacy of intracellular signalling, the high R_m on distal dendrites enhances signal transfer for slow distal inputs in BCs.

In summary, the distinct non-uniformity of R_m in BCs, in particular the low perisomatic R_m , ensures fast kinetics of somatic EPSPs generated by fast inputs albeit at the cost of substantial attenuation for distal inputs. At the same time, the high R_m on distal dendrites increases the efficacy for distal inputs at low frequencies.

19.3 Discussion

19.3.1 *Inhomogeneity of R_m in BCs Enhances Transfer of Distal Slow Input to the Soma*

Our results show that BCs exhibit distinct passive membrane properties; in particular R_m is non-uniform along the somato-dendritic axis, with a high value on the distal dendrites and low in the perisomatic region. This finding deviates from the uniform R_m in DG GCs (Schmidt-Hieber et al. 2007) and CA3 pyramidal cells (Major et al. 1994) and is in stark contrast to the gradient observed in CA1 or neocortical pyramidal cells (Golding et al. 2005; Stuart and Spruston 1998).

How do these divergent distributions of R_m influence synaptic integration? We showed that in BCs the transfer resistance and thus the somatic response to synaptic inputs onto the dendrites are equalised over a wide range of distances (Fig. 19.4c, right, light blue). In contrast, if a uniform R_m is implemented the difference of transfer resistance between proximal and distal compartments is stronger (Fig. 19.4c, right, black). This effect is further enhanced if an opposite gradient of R_m is used, leading to an electrotonic separation of the distal dendritic tree from the soma as for example in the thin and distal apical tufts of pyramidal cell dendrites (London et al. 1999). Voltage-dependent conductances are required for local nonlinear integration and transmission of distal synaptic inputs to the soma, as observed in neocortical pyramidal neurons (Larkum et al. 2009). Since BCs show only minimal voltage-dependent conductances along their dendritic tree (Hu et al. 2010), the BC-type non-uniformity with high R_m in the distal dendrites appears to be optimised for the transmission of distal synaptic inputs down to the soma.

Consistent with the slow integrative properties of distal apical dendrites, the entorhinal input is primarily tuned to the low theta frequency range. Recent experimental evidence further suggests that theta activity from the entorhinal cortex at 10 Hz activates GCs most efficiently in the functional DG network (Ewell and Jones 2010). The proposed mechanism is that lower as well as higher frequencies lead to increased inhibition, whereas a frequency around 10 Hz leads to EPSP facilitation, efficient temporal summation and reduced inhibition in GCs. The non-uniform R_m in BCs could support such a mechanism. For low frequencies, inhibition in GCs by BCs is enhanced because of the more efficient signal transfer (see Fig. 19.4c, right) at distal apical dendrites. In contrast, at higher frequencies, proximal and basal inputs may preferentially recruit BCs and increase inhibition onto GCs.

19.3.2 *Fast Signalling in the Basal Dendrites of BCs*

BCs are well known for their fast synaptic and intrinsic properties. They have fast excitatory (Geiger et al. 1997) and inhibitory synaptic inputs (Bartos et al. 2001, 2002), fast membrane time constant (Jonas et al. 2004), fast discharge pattern (Pike et al.

2000) and fast synaptic output (Bucurenciu et al. 2008). These fast properties are important for the precise timing of principal discharge and the generation of gamma oscillations within the DG (Bartos et al. 2007). Our results further demonstrate that membrane properties, in particular the R_m , and the electrotonic structure appear to be also optimised to serve fast signalling in the basal dendrites and the perisomatic domain of these interneurons.

In fact, there are marked differences between apical and basal dendrites as well as proximal and distal synapses. These differences are consistent with the divergent properties of the synapses themselves: Inputs of the perforant path onto the distal apical BC dendrites express slower calcium-impermeable glutamate receptors of the AMPA type, whereas mossy fibre inputs onto the proximal basal BC dendrites express fast calcium-permeable AMPA receptors (Sambandan et al. 2010). Our results further show that EPSPs on apical dendrites propagate slower and will have slower kinetics when reaching the soma than those on basal dendrites (Fig. 19.4b). Thus, the recurrent inputs onto the basal dendrites have a kinetic advantage over those onto the apical ones.

What might be the network impact of this kinetic advantage of the feedback circuit? The DG consists of $\sim 10^3$ – 10^4 times more GCs than BCs, and the divergent GC–BC connectivity is smaller than the convergent BC–GC connection (Patton and McNaughton 1995). As soon as GCs are activated by entorhinal inputs, they can recruit BCs in a fast and reliable manner, thereby producing strong feedback inhibition to the GC population. The strong inhibitory feedback and the lack of recurrent excitatory synapses (i.e. GC–GC synapses) make DG circuits a competitive network (Rolls and Treves 1998).

In such a network, sparse activity and a high signal-to-noise ratio can be achieved. Specifically in the DG, information flow could be as follows. The main input, the perforant path, is weak and slow and will not activate BCs but rather put them into a ready-to-fire subthreshold state. However, when a small set of highly excited GCs discharge, they can recruit BCs. Feedback inhibition will suppress any further activity in the GC population, maintaining the sparse activity pattern and a good signal-to-noise ratio. Synapses onto the “winner” GC could be potentiated under these conditions, whereas synapses onto suppressed GCs will not undergo potentiation or may even show depression. Thus, potentiated GCs can emerge as a cell assembly which transmits the given information further to CA3, consistent with a winner-takes-all mechanism.

The synaptic and dendritic properties of the basal dendrites involved in feedback inhibitory loop are central to these mechanisms, because they enable the fast, temporally precise and efficient activation of BCs by low number of coincident inputs (Geiger et al. 1997; Nörenberg et al. 2010). Furthermore, the GC-to-BC synapse might itself undergo potentiation in an associative manner under these conditions (Sambandan et al. 2010). The precise role of associative plasticity is not known, but one can speculate that on the one hand it will help to preserve the balance of excitation and inhibition in the circuit. On the other hand, it may facilitate the emergence and stabilise the “winner” cell assembly.

Although main aspects of computational function of the DG are becoming apparent, several details of the underlying microcircuit mechanisms are still unknown. In particular the role of the various types of interneurons, e.g. the distinct operation of dendrite-inhibiting versus perisomatic-inhibiting interneurons, remains elusive. Our results provide some insights into how the divergent properties of synaptic inputs and surface membranes of different subcellular compartments in BCs contribute to microcircuit operation in the DG. However, further systematic analysis of synaptic and integrative properties as well as the pattern and timing of activity of the various interneuron types will be required to better understand how inhibitory neurons contribute to the control of flow and storage of information in the DG and other cortical networks.

References

- Amaral DG (1993) Emerging principles of intrinsic hippocampal organization. *Curr Opin Neurobiol* 3(2):225–229
- Andersen P, Bliss TV, Skrede KK (1971) Lamellar organization of hippocampal pathways. *Exp Brain Res* 13(2):222–238
- Ascoli GA et al (2008) Petilla terminology: nomenclature of features of GABAergic interneurons of the cerebral cortex. *Nat Rev Neurosci* 9(7):557–568
- Bartos M, Vida I, Frotscher M et al (2001) Rapid signaling at inhibitory synapses in a dentate gyrus interneuron network. *J Neurosci* 21(8):2687–2698
- Bartos M, Vida I, Frotscher M et al (2002) Fast synaptic inhibition promotes synchronized gamma oscillations in hippocampal interneuron networks. *Proc Natl Acad Sci USA* 99(20):13222–13227
- Bartos M, Vida I, Jonas P (2007) Synaptic mechanisms of synchronized gamma oscillations in inhibitory interneuron networks. *Nat Rev Neurosci* 8(1):45–56
- Bartos M, Alle H, Vida I (2011) Role of microcircuit structure and input integration in hippocampal interneuron recruitment and plasticity. *Neuropharmacology* 60(5):730–739
- Brent RP (2002) Algorithms for minimization without derivatives. Dover Publications, Mineola, NY
- Bucurenciu I, Kulik A, Schwaller B et al (2008) Nanodomain coupling between Ca²⁺ channels and Ca²⁺ sensors promotes fast and efficient transmitter release at a cortical GABAergic synapse. *Neuron* 57(4):536–545
- Buzsáki G (2006) Rhythms of the brain. Oxford University Press, New York, NY
- Buzsáki G, Draguhn A (2004) Neuronal oscillations in cortical networks. *Science* 304(5679):1926–1929
- Carnevale NT, Hines ML (2006) The NEURON book. Cambridge University Press, Cambridge
- Chitwood RA, Hubbard A, Jaffe DB (1999) Passive electrotonic properties of rat hippocampal CA3 interneurons. *J Physiol* 515(Pt 3):743–756
- Ewell LA, Jones MV (2010) Frequency-tuned distribution of inhibition in the dentate gyrus. *J Neurosci* 30(38):12597–12607
- Fisahn A, Yamada M, Duttaroy A et al (2002) Muscarinic induction of hippocampal gamma oscillations requires coupling of the M1 receptor to two mixed cation currents. *Neuron* 33(4):615–624
- Förster E, Zhao S, Frotscher M (2006) Laminating the hippocampus. *Nat Rev Neurosci* 7(4):259–267
- Freund TF, Buzsáki G (1996) Interneurons of the hippocampus. *Hippocampus* 6(4):347–470

- Geiger JR, Lübke J, Roth A et al (1997) Submillisecond AMPA receptor-mediated signaling at a principal neuron-interneuron synapse. *Neuron* 18(6):1009–1023
- Gentet LJ, Stuart GJ, Clements JD (2000) Direct measurement of specific membrane capacitance in neurons. *Biophys J* 79(1):314–320
- Golding NL, Mickus TJ, Katz Y et al (2005) Factors mediating powerful voltage attenuation along CA1 pyramidal neuron dendrites. *J Physiol* 568(Pt 1):69–82
- Gulledge AT, Kampa BM, Stuart GJ (2005) Synaptic integration in dendritic trees. *J Neurobiol* 64(1):75–90
- Gulyás AI, Buzsáki G, Freund TF et al (2006) Populations of hippocampal inhibitory neurons express different levels of cytochrome c. *Eur J Neurosci* 23(10):2581–2594
- Hille B (2001) Ion channels of excitable membranes. Sinauer Associates Inc, Sunderland
- Hines ML, Carnevale NT (1997) The NEURON simulation environment. *Neural Comput* 9(6):1179–1209
- Hu H, Martina M, Jonas P (2010) Dendritic mechanisms underlying rapid synaptic activation of fast-spiking hippocampal interneurons. *Science* 327(5961):52–58
- Jonas P, Bischofberger J, Fricker D et al (2004) Interneuron diversity series: fast in, fast out—temporal and spatial signal processing in hippocampal interneurons. *Trends Neurosci* 27(1):30–40
- Koch C (1999) Biophysics of computation. Oxford Univ Press, Oxford
- Krueppel R, Remy S, Beck H (2011) Dendritic integration in hippocampal dentate granule cells. *Neuron* 71(3):512–528
- Larkum ME, Nevian T, Sandler M et al (2009) Synaptic integration in tuft dendrites of layer 5 pyramidal neurons: a new unifying principle. *Science* 325(5941):756–760
- Lewis DA, Hashimoto T, Volk DW (2005) Cortical inhibitory neurons and schizophrenia. *Nat Rev Neurosci* 6(4):312–324
- London M, Meunier C, Segev I (1999) Signal transfer in passive dendrites with nonuniform membrane conductance. *J Neurosci* 19(19):8219–8233
- Losonczy A, Magee JC (2006) Integrative properties of radial oblique dendrites in hippocampal CA1 pyramidal neurons. *Neuron* 50(2):291–307
- Magee JC (2000) Dendritic integration of excitatory synaptic input. *Nat Rev Neurosci* 1(3):181–190
- Major G, Larkman AU, Jonas P et al (1994) Detailed passive cable models of whole-cell recorded CA3 pyramidal neurons in rat hippocampal slices. *J Neurosci* 14(8):4613–4638
- Nörenberg A, Hu H, Vida I et al (2010) Distinct nonuniform cable properties optimize rapid and efficient activation of fast-spiking GABAergic interneurons. *Proc Natl Acad Sci USA* 107(2):894–899
- Patton PE, McNaughton B (1995) Connection matrix of the hippocampal formation: I. The dentate gyrus. *Hippocampus* 5(4):245–286
- Pike FG, Goddard RS, Suckling JM et al (2000) Distinct frequency preferences of different types of rat hippocampal neurones in response to oscillatory input currents. *J Physiol* 529(Pt 1):205–213
- Rall W (1959) Branching dendritic trees and motoneuron membrane resistivity. *Exp Neurol* 1:491–527
- Rall W (1962) Electrophysiology of a dendritic neuron model. *Biophys J* 2(2 Pt 2):145–167
- Rolls ET, Treves A (1998) The hippocampus and memory. In: Rolls ET, Treves A (eds) Neural networks and brain function. Oxford University Press, New York, NY, pp 118–120
- Sambandan S, Sauer JF, Vida I et al (2010) Associative plasticity at excitatory synapses facilitates recruitment of fast-spiking interneurons in the dentate gyrus. *J Neurosci* 30(35):11826–11837
- Schmidt-Hieber C, Jonas P, Bischofberger J (2007) Subthreshold dendritic signal processing and coincidence detection in dentate gyrus granule cells. *J Neurosci* 27(31):8430–8441
- Scott LL, Mathews PJ, Golding NL (2005) Posthearing developmental refinement of temporal processing in principal neurons of the medial superior olive. *J Neurosci* 25(35):7887–7895
- Spruston N, Stuart G, Häusser M (2008) Dendritic integration. In: Stuart G, Spruston N, Häusser M (eds) Dendrites, 2nd edn. Oxford University Press, Oxford, pp 231–270

- Stuart G, Spruston N (1998) Determinants of voltage attenuation in neocortical pyramidal neuron dendrites. *J Neurosci* 18(10):3501–3510
- Thurbon D, Lüscher HR, Hofstetter T et al (1998) Passive electrical properties of ventral horn neurons in rat spinal cord slices. *J Neurophysiol* 79(5):2485–2502
- Vetter P, Roth A, Häusser M (2001) Propagation of action potentials in dendrites depends on dendritic morphology. *J Neurophysiol* 85(2):926–937
- Vida I, Bartos M, Jonas P (2006) Shunting inhibition improves robustness of gamma oscillations in hippocampal interneuron networks by homogenizing firing rates. *Neuron* 49(1):107–117
- Whittington MA, Traub RD, Jefferys JG (1995) Synchronized oscillations in interneuron networks driven by metabotropic glutamate receptor activation. *Nature* 373(6515):612–615